Journal of Advanced Marine Engineering and Technology, Vol. 49, No. 2, pp. 77~83, 2025
J. Advanced Marine Engineering and Technology (JAMET)
https://doi.org/10.5916/jamet.2025.49.2.77

ISSN 2234-7925 (Print)
ISSN 2765-4796 (Online)
Original Paper

Evaluation of hydrogen embrittlement in notched STS 310S using electrochemical hydrogen charging

Byeong-Kwan Hwang[1] · Seung-Joo Cha[2] · Hyeon-Woo Choi[3] · Jeong-Hyeon Kim[4] · Jae-Myung Lee[†]

(Received April 4, 2025 ; Revised April 13, 2025 ; Accepted April 22, 2025)

Abstract: While hydrogen has garnered attention as a clean energy source, its interaction with metals can lead to hydrogen embrittlement, potentially compromising structural integrity. In this study, slow strain-rate tensile tests were conducted under both ex-situ and in-situ electrochemical hydrogen charging conditions to investigate the hydrogen embrittlement behavior of STS 310S. The results showed that ex-situ charging minimized the mechanical degradation due to hydrogen desorption, whereas in-situ charging significantly reduced the notch tensile strength and elongation. Nevertheless, STS 310S exhibits excellent resistance to hydrogen embrittlement. Additionally, a thermal desorption analysis was performed to quantify the absorbed hydrogen concentration, with the diffusion mechanism evaluated based on Fick's second law. The calculated hydrogen concentration profile indicated that the diffusion was primarily concentrated near the surface, potentially affecting the mechanical performance in localized regions.

Keywords: STS 310S, Hydrogen embrittlement, Electrochemical hydrogen Charging, Slow strain rate test

1. Introduction

With the continuous increase in global energy demand, concerns about environmental pollution have intensified. To address these issues, a transition to sustainable and eco-friendly alternative energy sources is essential. Among these alternatives, liquefied natural gas (LNG) and hydrogen have attracted significant attention, with hydrogen considered a clean energy source that emits little to no pollutants **[1]**.

However, hydrogen is highly soluble in metals and can lead to a phenomenon known as hydrogen embrittlement—characterized by the loss of ductility and fracture resistance in metals caused by the infiltration of hydrogen, which alters the microstructure and potentially causes unexpected structural failure **[2]**. Furthermore, hydrogen interacts with microstructural features such as grain boundaries, dislocations, and twins, promoting crack initiation in regions with localized stress concentration **[3][4]**. Hydrogen embrittlement poses a significant concern for the reliability and safety of structures, making it a critical factor in the design and operation of hydrogen-based systems.

Austenitic stainless steel is known for its relatively high stability and resistance to hydrogen embrittlement in hydrogen environments. This resistance is attributed to the low hydrogen diffusivity and high hydrogen solubility, which reduce the likelihood of hydrogen-induced cracking **[5]**. Owing to these properties, many researchers have studied the hydrogen embrittlement susceptibility of austenitic stainless steels under various conditions.

Sung *et al.* (2023) compared the effects of hydrogen embrittlement on STS 316 L, STS 304, and SS400 using electrochemical hydrogen charging. The results showed that STS 316 L exhibited almost no degradation in mechanical performance after hydrogen charging, STS 304 exhibited a slight reduction in elongation, and SS400 experienced a significant decline in mechanical properties **[6]**. Hwang *et al.* (2019) evaluated the hydrogen embrittlement susceptibility of STS 304 L under electrochemical hydrogen charging using the charging time and crosshead speed as variables. This study revealed that longer charging times and slower crosshead speeds led to increased hydrogen embrittlement sensitivity **[7]**. Kim *et al.* (2022) conducted tensile tests on hydrogen-charged and uncharged STS 304 L and 316 L specimens under

† Corresponding Author (ORCID: http://orcid.org/0000-0002-8096-4306): Professor, Department of Naval Architecture and Ocean Engineering, Pusan National University, 2, Busandaehak-ro 63beon-gil, Geumjeong-gu, Busan 46241, Korea E-mail: jaemlee@pusan.ac.kr, Tel: 051-510-2342
1 Ph. D. Candidate, Dept. of Naval Architecture and Ocean Engineering, Pusan National University, E-mail: byeongkwan_h@pusan.ac.kr Tel: 051-510-2340
2 Ph. D. Candidate, Dept. of Naval Architecture and Ocean Engineering, Pusan National University, E-mail: tmdwn219@pusan.ac.kr Tel: 051-510-2340
3 M. S. Candidate, Dept. of Naval Architecture and Ocean Engineering, Pusan National University, E-mail: rookie7533@pusan.ac.kr Tel: 051-510-2340
4 Professor, Hydrogen Ship Technology Center, Pusan National University, E-mail: jeonghkim@pusan.ac.kr Tel: 051-510-7953

30 mA/cm² current density at 300 K and 20 K. The results showed no significant differences in the yield strength and tensile strength between the hydrogen-charged and uncharged specimens **[8]**. Wang *et al.* (2018) performed electrochemical hydrogen charging at a current density of 1.1 mA/cm^2 and analyzed the tensile behavior of pre-strained and non-pre-strained 304 L and 316 L stainless steels. The hydrogen embrittlement index was 6% for 304 L and 2% for 316 L in the specimens without prestraining **[9]**.

Most previous studies have employed the ex-situ hydrogen charging method, in which hydrogen is charged into the material before testing. However, this approach can lead to the release of hydrogen gas during testing, resulting in a nonuniform hydrogen distribution within the material **[10]**. Thus, performing testing under in-situ hydrogen charging conditions, where hydrogen is continuously supplied during testing, is necessary to achieve a more uniform hydrogen distribution **[11]**.

Therefore, in this study, slow strain rate tensile tests were conducted on notched STS 310S specimens under both ex-situ and in-situ hydrogen-charging conditions. In addition, tests were performed under various current-density conditions to analyze the effects of hydrogen on the mechanical behavior of STS 310S.

2. Experimental Preparation

2.1 Specimen Preparation

The geometry of the STS 310S notched tensile specimen used in the slow strain rate tensile test is shown in **Figure 1**. The chemical composition of the specimens (based on weight percentage) was 0.046% C, 0.53% Si, 1.80% Mn, 0.023% P, 0.001% S, 19.1% Ni, and 24.3% Cr. The specimen was machined from a plate and finalized into a tensile specimen with a notch radius of 0.1 mm, gauge length of 50 mm, and thickness of 3 mm.

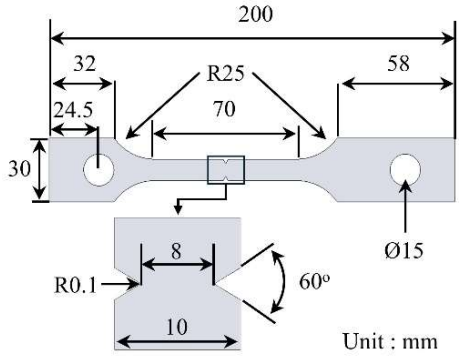

Figure 1: Geometry of the notched tensile specimen

2.2 Electrochemical Hydrogen Charging

Electrochemical hydrogen charging was performed using an aqueous solution containing 3 wt.% NaCl and 0.3 wt.% ammonium thiocyanate in accordance with ISO 16573 **[12]**. A platinum mesh was used as the anode, and a specimen was used as the cathode.

For ex-situ hydrogen charging, high current densities of 10, 30, and 50 mA/cm^2 were applied to account for hydrogen desorption. In contrast, under the in-situ hydrogen charging conditions, current densities of 0.5, 1, 5, and 10 mA/cm^2 were applied.

2.3 Slow Strain Rate Test

To evaluate the hydrogen embrittlement susceptibility of STS 310S, slow strain rate tensile tests were conducted under both ex-situ and in-situ hydrogen charging conditions. The tests were performed at room temperature using a universal testing machine at a constant strain rate of 3×10^{-5} /s. The specimen displacements were measured using an extensometer with a gauge length of 50 mm.

Before the test, the specimens for ex-situ hydrogen charging were precharged for 72 h in accordance with ISO 16573 **[12]**. Under in-situ conditions, hydrogen was continuously supplied during the test to prevent desorption.

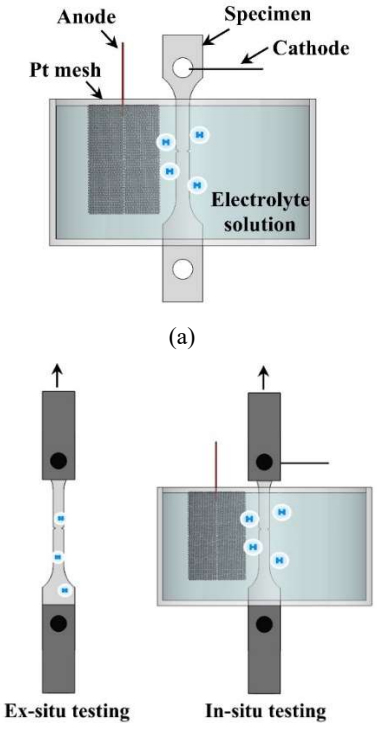

Figure 2: Schematic diagram: (a) Hydrogen pre-charging; (b) Ex-situ and in-situ slow strain rate tensile tests

Each test was repeated thrice under the same conditions to ensure the reliability of the experimental results. A schematic illustration of the hydrogen pre-charging process and slow strain-rate tensile test setup for both the ex-situ and in-situ conditions is shown in **Figure 2**.

2.4 Hydrogen Concentration Analysis

The total hydrogen concentration in the specimens was measured using an ONH analyzer (ONH2000). The specimens had dimensions of 5 × 5 × 3 mm. This analyzer can detect hydrogen concentrations in the 0.01–1000 ppm range. The specimens were immediately stored on dry ice following electrochemical hydrogen charging to prevent hydrogen desorption, and the hydrogen concentration was measured within 30 min. During the analysis, each specimen was rapidly melted in a high-purity graphite crucible at temperatures exceeding 2000 ℃ using a pulse furnace. The thermally released hydrogen gas was transported by a stream of high-purity inert gas through a copper catalyst to remove interfering gases such as oxygen and nitrogen. The purified hydrogen was quantified using a thermal conductivity detector.

3. Results and Discussion

3.1 Results of Slow Strain Rate Tensile Tests

Figure 3 shows the stress–strain curves obtained from slow strain rate tensile tests conducted on notched STS 310S specimens under both ex-situ and in-situ hydrogen-charging conditions.

As shown in **Figure 3(a)**, under ex-situ hydrogen charging, the notched tensile strength and elongation were similar to those of the uncharged specimen, even when subjected to different applied current densities (10, 30, and 50 mA/cm^2), suggesting that the effect of hydrogen on the mechanical properties was limited under ex-situ conditions owing to hydrogen desorption during testing.

However, as shown in **Figure 3(b)**, under in-situ hydrogen charging conditions, the mechanical properties deteriorated with increasing current density. Both the notched tensile strength and elongation gradually decreased from 0.5 mA/cm^2 to 5 mA/cm^2, beyond which the values plateaued, showing minimal variation at 10 mA/cm^2.

This result suggests that STS 310S reaches a saturation level of hydrogen-induced degradation of its mechanical properties at current densities above 5 mA/cm^2. This behavior implies that fracture in hydrogen environments occurs when a certain critical

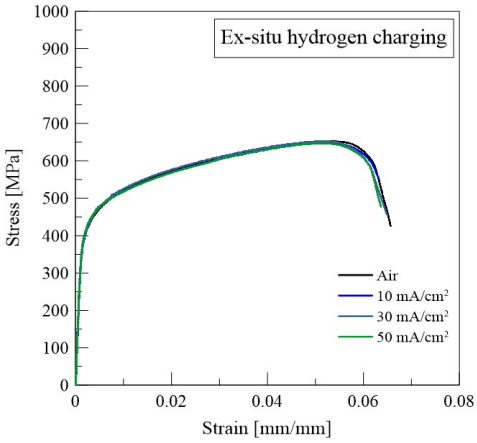

(a)

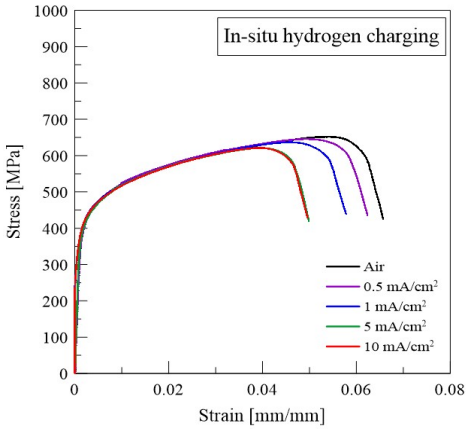

(b)

Figure 3: Stress–strain curves at different current densities: (a) Ex-situ and (b) in-situ hydrogen charging

hydrogen concentration is reached; beyond that point, additional hydrogen charging has a limited effect on mechanical performance. The test results indicate that hydrogen embrittlement susceptibility varies depending on the hydrogen charging method; thus, the influence of the charging conditions should be carefully considered in hydrogen embrittlement evaluations.

3.2 Evaluation of Hydrogen Embrittlement Susceptibility

Hydrogen embrittlement susceptibility is typically evaluated based on the extent to which the notched tensile strength decreases in a hydrogen-charged environment compared with that in an uncharged (air) condition **[13]**. In this study, the hydrogen embrittlement index (HE index) was defined as the ratio of the notched tensile strength in a hydrogen environment to that measured in air, referred to as the relative notch tensile strength.

Figure 4 shows the HE index of the STS 310S specimens under various current densities for both the ex-situ and in-situ hydrogen charging conditions.

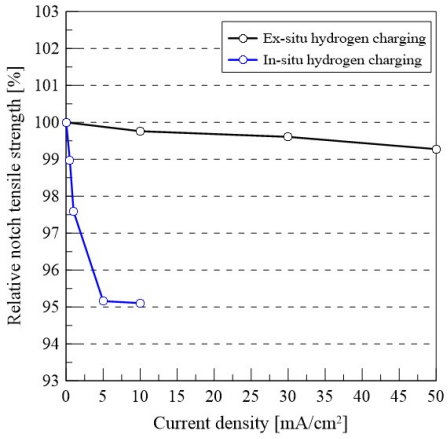

Figure 4: Relative notch tensile strength of STS 310S at different current densities: (a) Ex-situ and (b) in-situ hydrogen charging

The notched tensile strength of the uncharged STS 310S specimen was measured to be approximately 652.2 MPa. Even after hydrogen charging at current densities of 10, 30, and 50 mA/cm^2 under ex-situ conditions, the notched tensile strength remained as high as approximately 647.4 MPa. Despite the increase in current density, the mechanical performance exhibited negligible variation, and as a result, the HE index maintained values exceeding 99% at all tested current densities. These results indicate that, under ex-situ hydrogen charging, the degradation of the mechanical properties due to hydrogen embrittlement was minimal.

In contrast, under in-situ hydrogen charging, the notched tensile strength begins decreasing at a current density of 0.5 mA/cm^2, reaching approximately 645 MPa. It further decreased to approximately 621 MPa at 5 mA/cm^2 and remained at a similar level (620 MPa) at 10 mA/cm^2. However, even at the highest current density of 10 mA/cm^2, the HE index was maintained at approximately 95%.

This behavior is consistent with the properties of austenitic stainless steels, which exhibit low hydrogen diffusivity and high hydrogen solubility. These characteristics help confine hydrogen near the surface while limiting its penetration into the bulk material.

In particular, the high chromium (24.3 wt.%) and nickel (19.1 wt.%) content of STS 310S plays a critical role in enhancing hydrogen embrittlement resistance by improving the stability of the austenitic phase. These alloying elements stabilize the face-centered cubic (FCC) structure, thereby suppressing deformation-induced phase transformations, such as martensitic transformation, which is associated with increased resistance to hydrogen embrittlement **[14]**.

Moreover, chromium and nickel contribute to the reduction of hydrogen trapping at microstructural defects, such as dislocations and grain boundaries, which are potential nucleation sites for crack initiation. By minimizing these hydrogen-trapping effects, the alloy maintained its ductility and fracture resistance, even under hydrogen-rich conditions. Previous studies have shown that high Cr-Ni austenitic steels suppress phase transformations and hydrogen-assisted cracking more effectively than low-alloy steels **[15]**.

Accordingly, STS 310S demonstrated superior mechanical performance and structural stability in both ex-situ and in-situ hydrogen environments.

3.3 Hydrogen Concentration Analysis

The amounts of hydrogen charged at each current density via electrochemical hydrogen charging are summarized in **Table 1**. As the current density increased, the hydrogen concentration also increased. However, above 10 mA/cm^2, the rate of increase was more gradual. This behavior was presumed to be due to the saturation of the electrochemical reaction at higher current densities, which led to a decrease in the hydrogen charging efficiency.

Hydrogen is generally known to initiate at the metal surface and diffuse inwards. Accordingly, the hydrogen concentration distribution was calculated based on Fick's second law of diffusion, as defined by **Equation (1) [16]**.

$$C(x) = C_s(1 - erf\left(\frac{x}{2\sqrt{Dt}}\right)) \quad (1)$$

where $C(x)$ is the hydrogen concentration at depth x (wppm); C_s is the surface hydrogen concentration (wppm); D is the hydrogen diffusion coefficient (m^2/s) defined in **Equation (2) [17]**; t is the hydrogen charging time (s); erf is the error function.

$$D = 8.9 \times 10^{-7} exp\ (-\frac{E_B}{RT}) \quad (2)$$

where E_B is the activation energy for hydrogen diffusion (53.9 kJ/mol), R is the universal gas constant for hydrogen (8.314 J/mol·K), and T is the absolute temperature.

In this study, calculations were performed at room temperature (298 K). Assuming a surface hydrogen concentration of 1 wppm, the theoretically calculated hydrogen concentration distribution is presented in **Figure 5**.

The estimated hydrogen diffusion depth was approximately 35

μm. These results indicate that hydrogen tends to accumulate locally near the surface, with diffusion concentrated toward the surface region.

The hydrogen concentration measured in this study was determined based on the total volume of the analyzed specimen (75 mm^3). Hydrogen was assumed to diffuse uniformly across all surfaces of the specimen. Under this assumption, the volume into which the hydrogen diffused, excluding the central region (which remained uncharged), was calculated to be approximately 3.79 mm^3. Based on the principle of mass conservation, the average hydrogen concentration in the hydrogen-diffused region was calculated as shown in **Equation (3)**.

$$\bar{C}_H = \frac{\bar{C}_{total} \times V_{total}}{V_H} \tag{3}$$

where $\bar{C}_H$ is the average hydrogen concentration (wppm), $\bar{C}_{total}$ is the average hydrogen concentration of the entire specimen (wppm), V_{total} is the total volume of the specimen (mm^3), and V_H is the volume of diffused hydrogen (mm^3).

Based on **Equation (3)**, the average hydrogen concentration in the hydrogen-diffused region was calculated as shown in **Table 2**. Using these results, the surface hydrogen concentration was back-calculated according to the formula given in **Equation (1)**, as shown in **Equation (4)**.

$$C_s = \frac{\bar{C}_H}{\frac{1}{d}\int_0^d \left(1-\mathrm{erf}\left(\frac{x}{2\sqrt{Dt}}\right)\right)dx} \tag{4}$$

where d represents the depth of the hydrogen diffusion. Accordingly, the hydrogen concentration distribution curves for each current density were calculated using **Equation (1)**, as shown in **Figure 6**.

The results indicate that the surface hydrogen concentration increased as the current density increased, suggesting that a greater amount of hydrogen was concentrated near the metal surface, which may have enhanced the influence of hydrogen on embrittlement. In particular, a steeper concentration gradient near the surface implies that hydrogen diffusion is more localized, leading to a higher probability of hydrogen accumulation at microstructural defects such as grain boundaries, dislocations, or inclusions. This localized hydrogen enrichment can serve as an initiation site for microcracks under mechanical stress, thereby increasing susceptibility to hydrogen-assisted cracking. In addition, the limited diffusion depth observed across all current

Table 1: Measured hydrogen concentration at different current densities

Current density [mA/cm^2]	Hydrogen concentration [wppm]
0	0.05±0.01
0.5	24.90±0.53
1	27.33±0.45
5	33.94±0.78
10	37.25±0.84
30	43.18±0.66
50	46.25±0.71

Table 2: Average and surface hydrogen concentration in the diffused region at various current densities

Current density [mA/cm^2]	Average hydrogen concentration [wppm]	Surface hydrogen concentration [wppm]
0.5	492.7	1663.7
1	541.6	1828.4
5	672.8	2270.5
10	738.1	2490.5
30	859.4	2899.2
50	921.1	3107.1

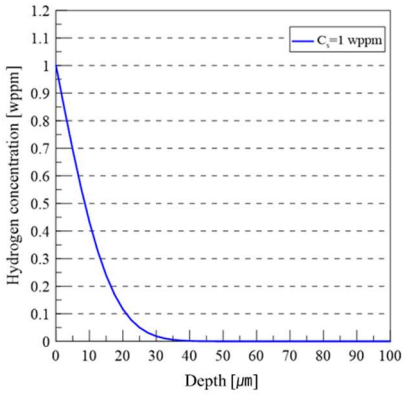

Figure 5: Hydrogen concentration profile assuming a surface hydrogen concentration of 1 wppm

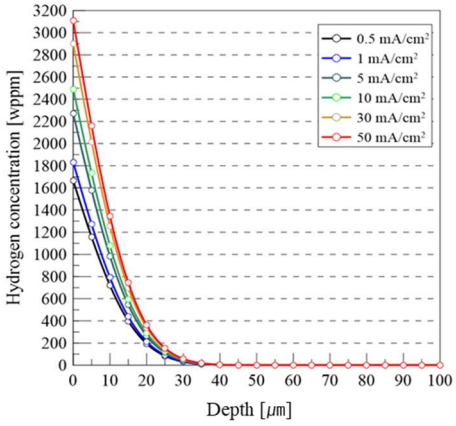

Figure 6: Hydrogen concentration profiles as a function of depth—calculated for various charging current densities

densities confirmed that hydrogen remained confined primarily to the near-surface region. This result indicates the importance of the surface geometry and regions with stress concentration, including notches, when evaluating hydrogen embrittlement behavior.

4. Conclusion

In this study, slow strain rate tensile tests were conducted on notched STS 310S specimens under electrochemical hydrogen charging conditions to quantitatively analyze their susceptibility to hydrogen embrittlement and hydrogen diffusion behavior.

The key findings are summarized as follows:

1. In the ex-situ hydrogen charging tests, the notched tensile strength and elongation exhibited minimal degradation, even at current densities of 10, 30, and 50 mA/cm^2—attributed to insufficient hydrogen accumulation in the material owing to desorption during testing.
2. Under in-situ hydrogen charging conditions, reductions in notched tensile strength and elongation were observed starting from a current density of 0.5 mA/cm^2, and damage due to hydrogen embrittlement appeared to saturate at current densities of 5 mA/cm^2 and above.
3. The HE index analysis showed values exceeding 99% under ex-situ conditions and above 95% under in-situ charging, indicating that STS 310S retains excellent mechanical stability in hydrogen environments.
4. The hydrogen concentration increased with current density; however, at current densities above 10 mA/cm^2, the rate of increase slowed owing to the decreased charging efficiency.
5. The hydrogen diffusion depth, calculated based on Fick's second law of diffusion, was estimated to be approximately 35 μm, suggesting that mechanical degradation is localized near the surface region.

These results provide a useful basis for quantitatively comparing hydrogen embrittlement susceptibility under ex-situ and in-situ charging conditions. Nevertheless, further studies are needed to evaluate the hydrogen embrittlement behavior of other stainless steels commonly used in industrial applications in comparison with STS 310S to investigate the influence of alloy composition. In addition, hydrogen embrittlement evaluations should be extended beyond the electrochemical charging method employed in this study to include more realistic operating conditions, such as high-pressure hydrogen gas environments.

Acknowledgement

This work was supported by Korea Institute for Advancement of Technology(KIAT) grant funded by the Korea Government(MOTIE) (RS-2023-KI002688, HRD Program for Industrial Innovation). This work was supported by the Materials/Parts Technology Development Program (20017575, Development of Applicability Evaluation Technology for Cryogenic Insulation Material and Storage Vessel considering Operating Condition of Hydrogen Commercial Vehicle) funded By the Ministry of Trade, Industry & Energy(MOTIE, Korea).

Author Contributions

Conceptualization, B. K. Hwang and S. J. Cha; Methodology, B. K. Hwang and H. W. Choi; Software, S. J. Cha; Formal Analysis, B. K. Hwang; Investigation, B. K. Hwang and J. H. Kim; Resources, B. K. Hwang; Data Curation B. K. Hwang and S. J. Cha; Writing-Original Draft Preparation, B. K. Hwang; Writing-Review & Editing, J. H. Kim; Visualization, H. W. Choi; Supervision, J. M. Lee; Project Administration, J. M. Lee; Funding Acquisition, J. H. Kim and J. M. Lee.

References

[1] K. W. Chun, "Technical guide for materials of containment system for hydrogen fuels for ships," Journal of Advanced Marine Engineering and Technology (JAMET), vol. 46, no. 5, pp. 212–217, 2022.

[2] Y. Song, S. Huang, J. Sheng, E. Agyenim-Boateng, Y. Jiang, Q. Liu, and M. Zhu, "Improvement of hydrogen embrittlement resistance of 2205 duplex stainless steel by laser peening," International Journal of Hydrogen Energy, vol. 48, no. 49, pp. 18930-18945, 2023.

[3] Y. Murakami, T. Kanezaki, and Y. Mine, "Hydrogen effect against hydrogen embrittlement," Metallurgical and Materials Transactions A, vol. 41, pp. 2548–2562, 2010.

[4] A. Campari, F. Ustolin, A. Alvaro, and N. Paltrinieri, "A review on hydrogen embrittlement and risk-based inspection of hydrogen technologies," International Journal of Hydrogen Energy, vol. 48, no. 90, pp. 35316–35346, 2023.

[5] L. Y. Mao, Z. A. Luo, C. Huang, Y. Q. Wang, R. H. Duan, and X. M. Zhang, "Effects of grain boundary character distribution on hydrogen-induced cracks initiation and propagation at different strain rates in a nickel-saving and high-

nitrogen austenitic stainless steel," Materials Science and Engineering: A, vol. 862, 144509, 2023.

[6] K. Y. Seong, J. H. Kim, J. H. Lee, and J. W. Lee, "Effect of hydrogen on stainless steel and structural steel using electrochemical charging facility," Journal of The Korean Society of Industry Convergence, vol. 26, no. 4, pp. 705–713, 2023 (in Korean).

[7] S. Hwang, S. Lee, J. Lee, D. Bae, M. Lee, and S. Nam, "Effect of hydrogen charging time and tensile loading speed on tensile properties of 304L stainless steels," Journal of The Korean Society of Industry Convergence, vol. 22, no. 1, pp. 11–20, 2019.

[8] M. S. Kim, T. Lee, Y. Son, J. Park, M. Kim, H. Eun, *et al.*, "Metallic material evaluation of liquid hydrogen storage tank for marine application using a tensile cryostat for 20 K and electrochemical cell," Processes, vol. 10, no. 11, p. 2401, 2022.

[9] Y. Wang, X. Wu, and W. Wu, "Effect of α′ martensite content induced by tensile plastic prestrain on hydrogen transport and hydrogen embrittlement of 304L austenitic stainless steel," Metals, vol. 8, no. 9, p. 660, 2018.

[10] D. Wang, A. B. Hagen, P. U. Fathi, M. Lin, R. Johnsen, and X. Lu, "Investigation of hydrogen embrittlement behavior in X65 pipeline steel under different hydrogen charging conditions," Materials Science and Engineering: A, vol. 860, p. 144262, 2022.

[11] H. Yu, A. Díaz, X. Lu, B. Sun, Y. Ding, M. Koyama, *et al.*, "Hydrogen embrittlement as a conspicuous material challenge—comprehensive review and future directions," Chemical Reviews, vol. 124, no. 10, pp. 6271–6392, 2024.

[12] ISO, "Steel — Measurement method for the evaluation of hydrogen embrittlement resistance of high strength steels — Part 1: Constant load test," Switzerland, ISO 16573-1, 2020.

[13] S. Corsinovi, L. Bacchi, M. Mastroianni, N. Bigollo, and R. Valentini, "Hydrogen embrittlement in high strength fasteners: comparison between bainitic and tempered martensitic steels," Engineering Failure Analysis, vol. 152, 107474, 2023.

[14] M. Martin, S. Weber, W. Theisen, T. Michler, and J. Naumann, "Effect of alloying elements on hydrogen environment embrittlement of AISI type 304 austenitic stainless steel," International Journal of Hydrogen Energy, vol. 36, no. 24, pp. 15888–15898, 2011.

[15] S. Ohmiya and H. Fujii, "Effects of Ni and Cr contents on fatigue crack growth properties of SUS316-based stainless steels in high-pressure gaseous hydrogen," ISIJ International, vol. 52, no. 2, pp. 247–254, 2012.

[16] M. Duportal, A. Oudriss, X. Feaugas, and C. Savall, "On the estimation of the diffusion coefficient and distribution of hydrogen in stainless steel," Scripta Materialia, vol. 186, pp. 282–286, 2020.

[17] C. San Marchi, B. P. Somerday, and S. L. Robinson, "Permeability, solubility and diffusivity of hydrogen isotopes in stainless steels at high gas pressures," International Journal of Hydrogen Energy, vol. 32, no. 1, pp. 100–116, 2007.